Research Article | Vol. 27, No. 10 | 13 May 2019 | OPTICS EXPRESS 14472
Optics EXPRESS

Optimal triplicator design applied to a geometric phase vortex grating

DAVID MARCO,[1] MARÍA M. SÁNCHEZ-LÓPEZ,[1] AARÓN COFRÉ,[2,3] ASTICIO VARGAS,[2] AND IGNACIO MORENO[3,*]

[1]*Instituto de Bioingeniería, Departamento de Física Aplicada, Universidad Miguel Hernández de Elche, 03202 Elche, Spain*
[2]*Departamento de Ciencias Físicas, Universidad de La Frontera, Temuco, Chile*
[3]*Departamento de Ciencia de Materiales, Óptica y Tecnología Electrónica, Universidad Miguel Hernández de Elche, 03202 Elche, Spain*
**i.moreno@umh.es*

Abstract: In this work, a geometric phase liquid-crystal diffraction grating based on the optimal triplicator design is realized, i.e., a phase-only profile that generates three diffraction orders with equal intensity and maximum diffraction efficiency. We analyze the polarization properties of this special diffraction grating and then use embedded spiral phases to design geometric phase vortex diffraction gratings. Finally, the fabrication of a two-dimensional version of such a design using a micro-patterned half-wave retarder is demonstrated, where the phase distribution is encoded as the orientation of the fast axis of the retarder. This proof-of-concept element is made of liquid crystal on BK7 substrate where the orientation of the LC is controlled via photoalignment, using a commercially available fabrication facility. Experimental results demonstrate the parallel generation of vortex beams with different topological charge and different states of polarization.

1. Introduction

The design and realization of diffraction gratings of evenly distributed intensity among a number of diffraction orders has been extensively studied. One initial approach that became very popular are Dammann gratings [1], which consist on gratings with a binary profile, where the transition points must be conveniently selected to provide the desired number of equally intense orders. Since then, this field continued to receive attention and applications such as diffractive elements for beam splitting and optical array illuminators were developed [2]. In 1998, Franco Gori and his associates introduced the analytical derivation of the optimal phase triplicator [3], a diffraction grating with a continuous phase-only profile that generates three diffraction orders (zero order and plus and minus first orders) with equal intensity and maximum diffraction efficiency. Although fabricating a grating with a continuous profile is more complicated than making binary profiles, the efficiency of Gori's design (about η = 93%) is very attractive, and the simplicity and beauty of its analytical expression makes it very easy to program and implement in a phase-only spatial light modulator (SLM) [4,5]. Some years after Gori's design, Romero and Dickey developed a generalized theory for designing continuous phase-only gratings that generate an arbitrary number of diffraction orders [6].

The interest of such grating profiles is not only limited to standard diffraction gratings. If combined with other phase functions (like those representing a lens or a helical plate), they can yield vortex gratings generating diffraction orders of different topological charges [7–9], or creating a three-dimensional array [10]. These vortex gratings have been extended to more complicated diffraction gratings in order to obtain vector beams. This is usually done by employing SLMs in different arrangements [11–13] to create the superposition of two beams with orthogonal polarizations and opposite vortex charge [14].

#360324 https://doi.org/10.1364/OE.27.014472
Journal © 2019 Received 15 Feb 2019; revised 15 Mar 2019; accepted 15 Mar 2019; published 6 May 2019

Optics EXPRESS

Despite the great flexibility that SLM offer, their use implies the realization of bulky systems. An alternative for making such elements more compact is based on encoding them as geometric phase (GP) elements, also known as Pancharatnam-Berry phase elements [15,16]. These are spatially variant half-wave retarders, where the orientation of the principal axis changes in-plane according to a given function. When illuminated with circularly polarized light, GP diffractive elements change the helicity of the circular polarization, but also imparts to the beam a phase function equal to twice the angular orientation of the retarder's principal axis. This way it is possible to create planar diffractive optical elements.

GP diffractive elements can be fabricated by photo-aligning liquid-crystals LC) [15,17]. LC based GP elements can be reconfigurable upon applying a voltage [18] and consequently the operating wavelength can be tuned. Instead, they can operate in a wide spectral range when based on cholesteric LC structures [19]. More complex designs involve not only controlling the orientation of the spatial retarder, but also the spatial variation of an additional phase, thus encoding two independent phase functions onto the two circular polarizations [20]. In this case, these elements are typically fabricated by nanostructuring metasurfaces [21]. While metamaterial-based GP elements are advantageous in terms of much higher energy damage threshold which renders them especially appropriate for operation with high-power lasers, LC based GP elements are easier to fabricate and represent a lower-cost method of fabrication. In fact, commercially available GP elements, such as vortex retarders and polarization sensitive lenses, can be exploited to design new optical systems [22]. In addition, some manufacturers offer the possibility to fabricate GP elements on demand, designed by the user.

This is the case in this work. Here we present the design and characterization of a special liquid-crystal GP diffraction grating. It creates a bidimensional array of 3 × 3 diffraction orders, obtained by combining two phase-only Gori's triplicators, one along the horizontal direction and another along the vertical direction. In addition, spiral phases of charges $\ell = 1$ and $\ell = 3$ are embedded in each direction. As a result, the grating generates in these nine diffraction orders vortex beams with topological charges that change from $\ell = -4$ to $\ell = +4$.

This diffraction grating is then fabricated as a GP diffractive element. For that purpose, we benefit from the facility provided by Thorlabs Inc. to fabricate customized liquid-crystal patterned retarders. These are composed of an array of microretarders with different orientation of the fast axis [23]. In our case, we ordered a custom half-wave retarder for the wavelength of 632.8 nm, where the axis alignment of the microretarders follow the above-mentioned diffraction grating profile. As a result, the designed grating is encoded as a GP diffraction grating. We demonstrate the expected array of vortex beams with different charges when the grating is illuminated with circular polarization. The polarization conversion is achieved when the grating is illuminated with circularly polarized light. When it is illuminated with linearly polarized light, however, the central order shows a different polarization conversion with respect to the lateral orders. We show that this a consequence of Gori's triplicator design, that includes a $\pi/2$ phase shift between the central order and the two lateral orders, which was not reported before. We note that a closely related design was presented recently in [24], where a 2D triplicator grating was combined with a spiral phase and fabricated as a GP metasurface. Our design differs, since it yields different charges onto different orders (opposed to the design in [24] where the same charge is obtained in the 3 × 3 diffraction orders).

The paper is organized as follows: after this Introduction, section 2 describes the grating's design, where a first part reviews Gori's triplicator. This scalar analysis is extended to a GP grating in Section 3, thus requiring a vector analysis that is based on the Jones matrix formalism. Section 4 describes the experimental system and discusses the experimental results, which demonstrate an excellent agreement with the expected results. Finally, Section 5 summarizes the conclusions of the work. The Appendix included at the end contains the required mathematical derivations for the sake of clarity.

Optics EXPRESS

2. The scalar grating design

In this section we describe the design of the phase vortex grating. First, we review Gori's design in a pure scalar treatment. Then we extend it to its application to a fork grating, i.e. a blaze grating with an embedded spiral phase. Finally, we describe the polarization effects when this grating profile is implemented as a geometric-phase diffractive element.

2.1. Gori's triplicator phase-only profile

As mentioned, in [3] Gori and his associates developed an analytical solution for the scalar phase-only triplicator, i.e., a diffraction grating exhibiting a continuous phase-only profile that generates three diffraction orders (zero and ± 1) of the same intensity and reaching the maximum diffraction. The phase profile they derived is given by

$$\phi(x) = \arctan\left[a\cos\left(\frac{2\pi x}{p}\right)\right], \tag{1}$$

where x denotes the transversal coordinate, p is the grating's period and a = 2.65718 is a numerical constant derived in [3]. We note here that in Gori's paper, the cosine function in Eq. (1) is instead a sine function, but this only implies a half period lateral displacement of the grating. We selected the cosine function in Eq. (1) because we found it simpler to analyze the Fourier spectrum, calculation that is presented in the Appendix of this manuscript.

The transmittance of the triplicator grating is given by

$$\tau_{trip}(x) = \exp\left[i\phi(x)\right] = \sum_{-\infty}^{+\infty}\tau_n \exp\left(in\frac{2\pi x}{p}\right), \tag{2}$$

where τ_n indicate the Fourier transform coefficients:

$$\tau_n = \frac{1}{p}\int_{-p/2}^{p/2}\exp\left[i\phi(x)\right]\exp\left(-in\frac{2\pi x}{p}\right)dx. \tag{3}$$

According to [3], the square magnitude of the three main diffraction orders is $|\tau_0|^2 = |\tau_{+1}|^2 = |\tau_{-1}|^2 = = 30.85\%$, rendering a total diffraction efficiency $\eta = |\tau_0|^2 + |\tau_{+1}|^2 + |\tau_{-1}|^2 = 92.56\%$. We note that this triplicator optimal efficiency is notably higher than that provided by the Dammann grating producing three diffraction orders, which is only of 66.42% [4,25].

Figure 1(a) shows three periods of the phase profile $\phi(x)$ given by Eq. (1) (black curve), which is compared with a linear blazed phase grating of the same period (blue curve). One interesting characteristic to note about Gori's triplicator profile is that the phase modulation changes from a minimum value of -0.39π to a maximum value of $+ 0.39\pi$, thus only requiring a total phase modulation of 0.78π to be perfectly displayed. Therefore, it is possible to implement it using SLM devices of very low phase levels [5]. Figure 1(b) illustrates the gray-level image that must be displayed onto a phase-only SLM to generate this triplicator.

Given the very reduced intensity of the diffraction orders different than order 0 and ± 1, we can consider that the triplicator merely generates these three diffraction orders (Fig. 1(c)) and Eq. (2) can be approximated as

$$\tau_{trip}(x) = \exp\left[i\phi(x)\right] \cong \tau_0 + \tau_{+1}\exp\left(i\frac{2\pi x}{p}\right) + \tau_{-1}\exp\left(-i\frac{2\pi x}{p}\right). \tag{4}$$

An important point that was not analyzed by Gori et al. in [3] is the relative phase shift between these three diffraction orders. In the Appendix, it is shown that there is a $\pi/2$ phase shift between the + 1 and −1 orders with respect to the zero order, hence, they hold the following relation

$$\tau_{+1} = \tau_{-1} = i\tau_0. \tag{5}$$

Optics EXPRESS

As we show later, this *i* factor has crucial impact when this design is implemented with geometric phase.

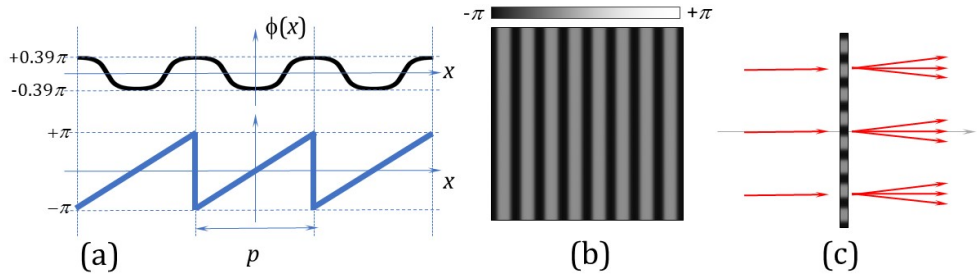

Fig. 1. (a) Gori's triplicator phase profile compared to the linear blaze grating profile. (b) Gray level image to generate a triplicator in a phase-only SLM. (c) Schematics of the triplication grating action.

2.2. The vortex triplicator grating

Figure 1(a) can be viewed as a phase look-up table (LUT) that assigns the phase of the triplicator profile to the corresponding phase value of the blazed (linear) profile, i.e.

$$\tau_{trip}(x) = \mathbf{LUT}\left[\tau_{linear}(x)\right], \tag{6}$$

where $\tau_{linear}(x) = \exp(i2\pi x/p)$. In this way, the phase LUT applies to all the phase values ranging from $-\pi$ to $+\pi$, and the triplicator design can be extended to more complex optical functions, different than a simple diffraction grating. An equivalent approach was applied for instance in [8] to binary phase Dammann grating profiles.

This is the case of the fork blazed phase grating. This grating is obtained by adding a spiral phase pattern to a linear blazed grating, whose transmittance is given by:

$$\tau_{fork}(x,\theta) = \exp\left[i\left(\frac{2\pi x}{p} + \ell\theta\right)\right]. \tag{7}$$

This phase-only function can be regarded as a blazed diffraction grating which generates a single first-order diffraction order that carries a vortex of charge ℓ. If this phase profile is modified, the other diffraction orders appear, with different topological charges. Different types of modifications of this blazed vortex grating have been demonstrated, including binary phase or Dammann grating type profiles [26–29].

By applying the LUT in Fig. 1(a) to this fork blazed grating, the optimum triplicator version of the fork grating is obtained. This is shown in Fig. 2. The addition modulo 2π of a linear phase grating and a spiral phase of charge $\ell = 1$, see Fig. 2(a), results in the classical fork phase-only grating as shown in Fig. 2(b). This grating, when illuminated with a plane wave, generates a single first order diffracted vortex beam that carries a topological charge $\ell = 1$. When the triplicator LUT is applied to this blazed vortex grating the resulting grating (Fig. 2(c)) shows the fork grating shape, but its profile adopts the form of the triplicator, as in Fig. 1(a)).

Mathematically, the application of the triplicator LUT results in the same Fourier series expansion as in Eq. (2), i.e.:

$$\tau_{trip-fork}(x,\theta) = \mathbf{LUT}\left[\tau_{fork}(x,\theta)\right] = \sum_{n=-\infty}^{+\infty}\tau_n \exp\left[in\left(\frac{2\pi x}{p} + \ell\theta\right)\right]. \tag{8}$$

To simplify the analysis, we consider only the diffracted orders $n_x = 0$, and $n_x = \pm 1$, all of them having the same magnitude $|\tau_{0,\pm 1}| = 0.555$ (equal intensities $|\tau_{0,\pm 1}|^2 = 0.3085$), but with a relative phase shift given by Eq. (5). Thus, within this approximation Eq. (8) can be written as

Optics EXPRESS

$$\tau_{trip-fork}(x,\theta)=\tau_0\left\{1+i\exp\left[i\left(\frac{2\pi x}{p}+\ell\theta\right)\right]+i\exp\left[-i\left(\frac{2\pi x}{p}+\ell\theta\right)\right]\right\}. \quad (9)$$

The first term in the right side of Eq. (9) corresponds to the zero order, with no topological charge. The other terms are two linear phases corresponding to the first and to the minus first diffraction orders, which carry charges ℓ and $-\ell$ respectively. Note that this grating diffracts in the horizontal direction. The above equation can be rewritten in a more compact way as

$$\tau_{trip-fork}(x,\theta)=\tau_0\left[1+2i\cos\left(\frac{2\pi x}{p}+\ell\theta\right)\right], \quad (10)$$

where the cosine term includes the $n_x = +1$ and $n_x = -1$ orders of charge ℓ and $-\ell$, respectively.

Next, another equivalent triplicator grating is designed, but now oriented to diffract in the vertical direction. For that purpose, we use another fork grating from a blazed grating of the same period and a spiral phase pattern with $\ell = 3$, as shown in Fig. 2(d). Its combination, shown in Fig. 2(e), is again modified according to the triplicator profile, resulting in the pattern in Fig. 2(f). This grating generates three diffraction orders in the vertical direction. Once again, the zero diffraction order does not have vorticity, but the vertically diffracted beams, $n_y = +1$ and $n_y = -1$, carry vortices of charges $\ell = 3$ and $\ell = -3$ respectively.

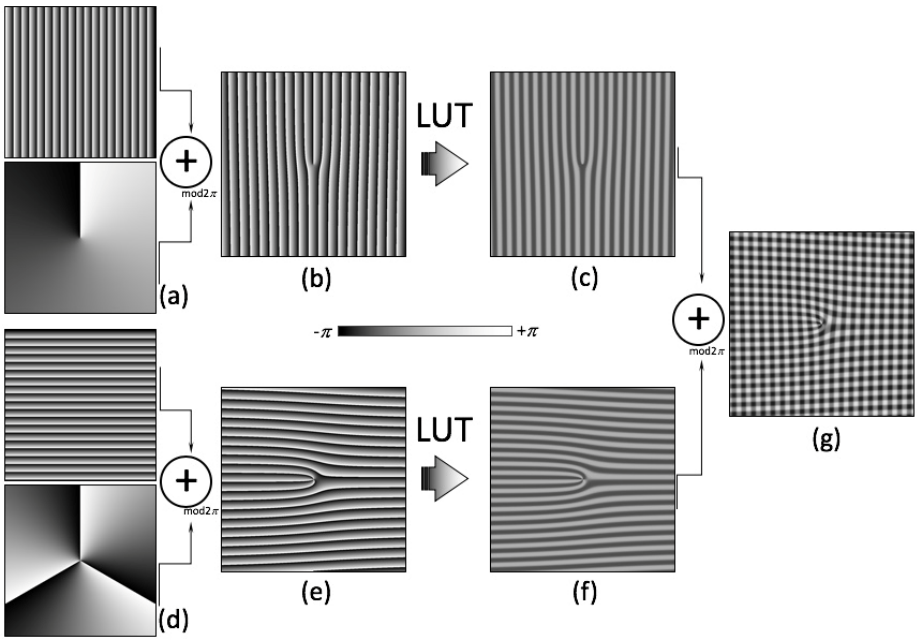

Fig. 2. Scheme showing the design procedure to achieve the 3x3 vortex grating design with optimal efficiency.

Finally, we combine both triplicator vortex gratings by making their product, i.e., by adding modulo 2π the two phase-only functions. The resulting phase pattern is a 2D diffraction grating as shown in Fig. 2(g), that creates an array of 3 × 3 diffraction orders, as shown in Fig. 3. The transmittance of this 2D grating is obtained from the multiplication of two terms like in Eq. (10) for the x and y directions:

$$\tau_{2D\,trip-fork}(x,y,\theta)=\tau_0^2\left[1+2i\cos\left(\frac{2\pi x}{p}+\theta\right)\right]\left[1+2i\cos\left(\frac{2\pi y}{p}+3\theta\right)\right], \quad (11)$$

Optics EXPRESS

where we made explicit the topological charges of 1 and 3 for the x and y directions respectively.

This product can be expanded to read as:

$$\frac{\tau_{2D\,trip-fork}(x,y,\theta)}{\tau_0^2}=1+2i\cos\left(\frac{2\pi x}{p}+\theta\right)-2\cos\left(\frac{2\pi(y-x)}{p}+2\theta\right)+ \\ 2i\cos\left(\frac{2\pi y}{p}+3\theta\right)-2\cos\left(\frac{2\pi(y+x)}{p}+4\theta\right) \tag{12}$$

The first unit term is the zero order, while each cosine term represents a pair of ± 1 diffraction orders. Note that the first and third cosine terms, which correspond to the orders diffracted along the horizontal (n_x = ± 1, n_y = 0) and vertical direction (n_x = 0, n_y = ± 1) respectively, are pure imaginary and therefore have a $\pi/2$ phase shift with respect to the zero order. On the contrary, the second and fourth cosine terms in Eq. (12), which correspond to the orders diffracted along the diagonal directions, are real. The second cosine term corresponds to the anti-diagonal diffraction orders (n_x = –1, n_y = + 1) and (n_x = + 1, n_y = –1), while the fourth cosine term corresponds to the diagonal orders, (n_x = n_y = + 1) and (n_x = n_y = –1).

Equation (12) also reveals that the topological charge changes on each diffraction order as

$$\ell(n_x,n_y)=n_x+3n_y, \tag{13}$$

where (n_x,n_y) are the pair of indices indicating the diffraction order (n_x,n_y = + 1,0,-1). Therefore the topological charges take values + 4, + 3…, 0,…-3, –4, at the nine diffraction orders. Figure 3 illustrates the array of 3 × 3 orders yielded by the grating design in Eq. (12), with indication of the topological charge at each diffraction order defined by the pair of indices (n_x,n_y).

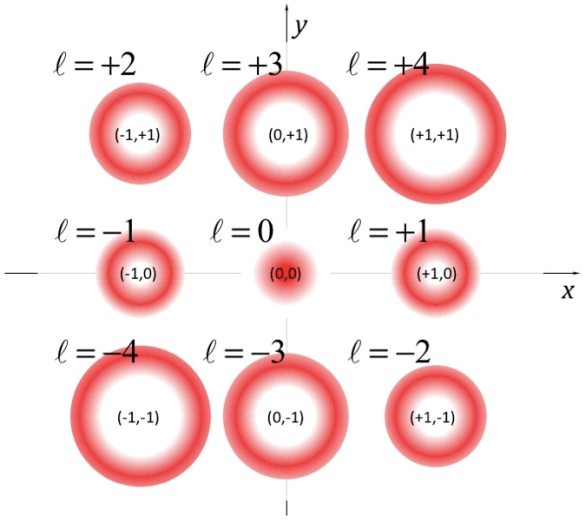

Fig. 3. Scheme of the expected array of diffraction orders and the corresponding topological charges. The pair of numbers on each diffraction order denote the order (n_x,n_y).

3. The geometric phase 2D vortex grating

In this work, we build the transmission profile of Eq. (12) as a geometric phase element, where the phase function $\phi(x,y)$ is encoded as the rotation angle α of the principal axis of a half-wave retarder. Figure 4(a) illustrates this method. The Jones matrix for a half-wave retarder with orientation α is given by:

Optics EXPRESS

$$\mathbf{M} = \begin{pmatrix} \cos 2\alpha & \sin 2\alpha \\ \sin 2\alpha & -\cos 2\alpha \end{pmatrix} \tag{14}$$

In a geometric phase element, α is a spatially-variant function given by $\alpha(x,y) = \phi(x,y)/2$ where ϕ is the phase to be encoded. Q-plates are a particular case where a spiral phase is encoded as geometric phase [30].

The above matrix can be expressed as:

$$\mathbf{M} = \frac{1}{2}\left(\mathbf{A}e^{i\phi} + \mathbf{A}^{\dagger}e^{-i\phi}\right), \tag{15}$$

with

$$\mathbf{A} = \begin{pmatrix} 1 & -i \\ -i & -1 \end{pmatrix}. \tag{16}$$

If we consider a phase-only function corresponding to a diffraction grating as those described above, $\tau(x,y) = \exp[i\phi(x,y)]$, it is convenient to write Eq. (15) in the following form:

$$\mathbf{M}(\tau) = \begin{pmatrix} 1 & 0 \\ 0 & -1 \end{pmatrix}\mathrm{Re}(\tau) + \begin{pmatrix} 0 & 1 \\ 1 & 0 \end{pmatrix}\mathrm{Im}(\tau). \tag{17}$$

Note that the Jones matrix acting on the real part of τ corresponds to a half-wave retarder (HWR) with its axis oriented along the coordinate system. On the contrary, the Jones matrix acting on the imaginary part of τ corresponds to an aligned HWR plus a rotation of 90°.

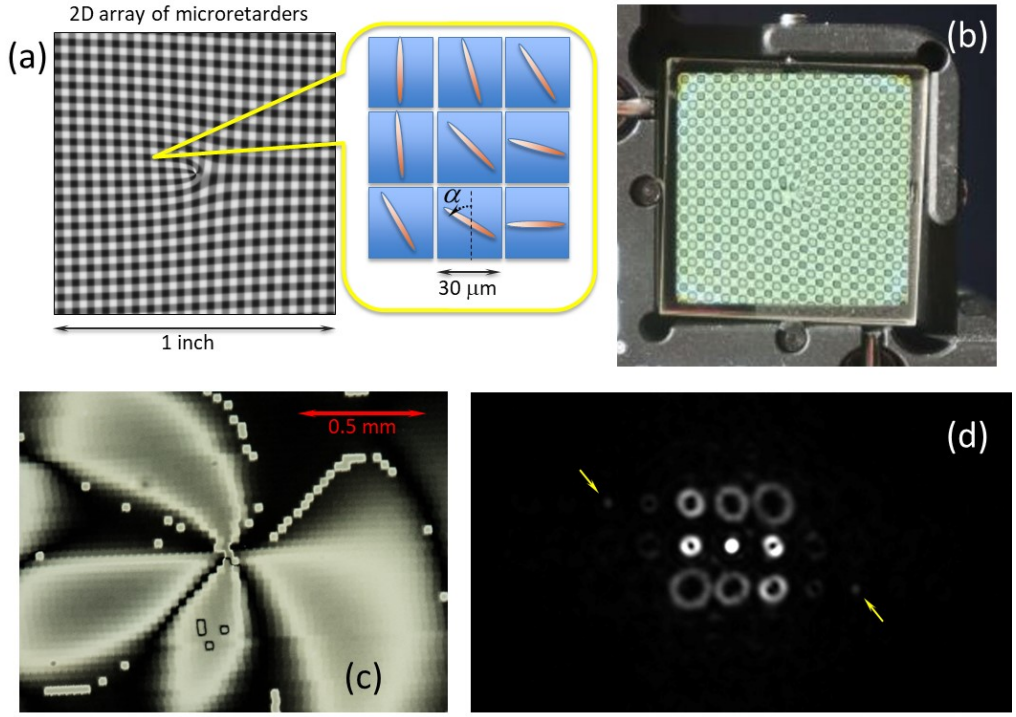

Fig. 4. (a) Illustration of the phase grating encoding as a geometric phase element. (b) Picture of the grating between crossed polarizers. (c) Detail of the center of the grating viewed through a polarizing microscope between crossed polarizers. (d) Fourier transform pattern, saturated on purpose in order to visualize how the energy is basically confined to the 3 × 3 target orders.

Thus, if we apply the geometric phase to the phase profile in Eq. (12), Eq. (17) is given by:

Optics EXPRESS

$$\mathbf{M}=\begin{pmatrix}1 & 0\\ 0 & -1\end{pmatrix}\times\left[1-2\cos\left(\frac{2\pi(y-x)}{p}+2\theta\right)-2\cos\left(\frac{2\pi(y+x)}{p}+4\theta\right)\right]+\\ \begin{pmatrix}0 & 1\\ 1 & 0\end{pmatrix}\times\left[2\cos\left(\frac{2\pi x}{p}+\theta\right)+2\cos\left(\frac{2\pi y}{p}+3\theta\right)\right] \quad (18)$$

Equation (18) reveals a different polarization behavior in two sets of diffraction orders. For those in the first row in Eq. (18) i.e., orders (+ 1, + 1), (–1, + 1), (0,0), (+ 1,-1) and (–1,-1), the polarization transformation induced by the grating is equivalent to an aligned HWR. On the contrary, for those orders described in the second row in Eq. (18), i.e., orders (1,0), (0,1), (–1,0) and (0,-1), the polarization transformation induced by the grating is equivalent to that of an aligned HWR plus a 90° polarization rotation.

4. Experimental system and results

We next show a proof-of-concept experiment where we use a geometric phase grating made using the capability offered by Thorlabs Inc. to provide customized patterned retarders [23]. The 2D vortex triplicator grating was fabricated as a patterned retarder with half-wave retardance for the wavelength of 632.8 nm. The complete element is composed of an array of 853 × 853 micro-retarders, each one of 30 × 30 μm^2, thus the grating size is about 1" × 1". The encoded grating was designed with a period p of 19 pixels. This large value was selected as a trade-off between having enough number of pixels per period to accurately reproduce the triplicator phase profile, and reaching a diffraction angle that, although small, is enough to separate the diffracted lowest vortex beams. Each micro-retarder has its fast axis aligned to a different angle, given by the designed phase mask. These patterned retarders are made of liquid crystals and liquid-crystal polymers and, using photo alignment technology, the fast axis of each micro-retarder can be oriented to any angle within a resolution of <1°. The grating was fabricated onto a BK7 substrate and with antireflection coating type A (for 350 - 700 nm), and it was mounted onto a square kinematic mount from Edmund Optics (model #58-860). Figure 4(b) shows a picture of the mounted grating, viewed between crossed polarizers, while Fig. 4(c) shows a detail of the central part viewed through a polarizing microscope (Nikon Eclipse). The picture shows the center of the grating where the singularity is created.

Let us now evaluate the diffraction pattern rendered by this grating. Figure 5 shows a scheme of the optical system. We use a 632.8 nm wavelength He-Ne laser beam that is spatially filtered and collimated. A quarter-wave retarder (Q) is used to generate circularly polarized light impinging on a polarization state generator (PSG) composed by a linear polarizer (P) and a quarter-wave retarder (Q). The PSG is applied in order to generate an arbitrary input state of polarization illuminating the geometric phase grating. Setting up the PSG requires changing the orientation of the polarizers; therefore, using circularly polarized light as input to the PSG ensures that the input intensity does not change when the PSG is reconfigured.

Optics EXPRESS

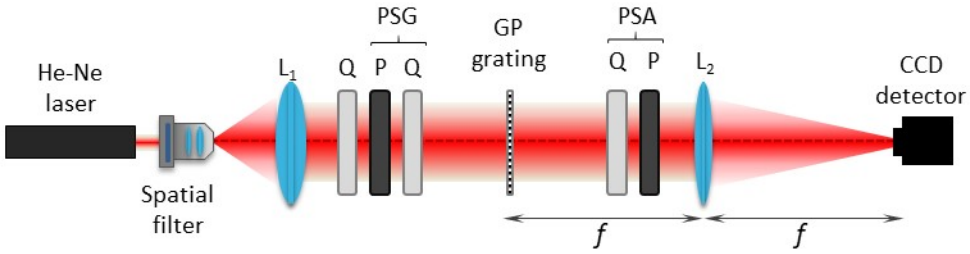

Fig. 5. Scheme of the experimental setup. PSG: polarization state generator; PSA: polarization state analyzer; Q: quarter-wave retarder; L: linear polarizer; L_1, L_2 converging lenses.

Behind the grating, a polarization state analyzer (PSA) composed by another quarter-wave plate and another linear polarizer is used to analyze the generated beams. A converging lens of f = 100 cm focal length focuses the beam onto a CCD detector that captures the Fourier transform pattern. Figure 4(d) shows a capture of the Fourier transform plane. This result was obtained with input linear polarization and no PSA. The 3 × 3 vortex beam array is successfully obtained, in agreement with the expected result in Fig. 3. The focused beams exhibit the typical doughnut shapes, with increasing diameter according to the topological charges in each diffraction order. Note, however, that we are operating at the limit, since the beams that focus with largest diameters (those with charges $\ell = \pm 3$ and $\ell = \pm 4$) are not completely separated and their interference causes some distortion. Nevertheless, this result represents a successful proof-of-concept of the vortex triplicator grating.

Figure 4(d) shows a big area of the Fourier transform pattern, which is saturated on purpose. This is done to clearly visualize that the energy is basically concentrated in the central array of 3 × 3 central orders. Other higher diffraction orders, although weak, are visible, especially those located at diffraction orders (+ 3,–1) and (–3, + 1), where the total topological charge is cancelled and therefore the focused beam appears as a bright spot (they are marked with a yellow arrow). We experimentally measured the intensity of the 3 × 3 central orders compared to the total intensity at the Fourier transform plane and obtained a ratio of about $\eta \approx 0.74$. This value is lower, but not far, from the theoretical efficiency of a 2D triplicator grating, $\eta = \eta_x \eta_y = (0.926)^2 = 0.857$, due to the limited spatial resolution in the fabrication of the grating.

In order to exhaustively analyze the polarization properties of the grating, Fig. 6 shows additional experimental results, where now only the central orders are shown. The PSG is configured to the six typical states used in polarimetry: linear states with orientations 0, ± 45° and 90°, and the two circular states right, and left. These polarization states are drawn as symbols on the left column in Fig. 6. For each PSG configuration, the PSA is first set without analyzer and is then set to transmit the six typical polarization states. These are indicated with the same symbols on the top of the figure.

Optics EXPRESS

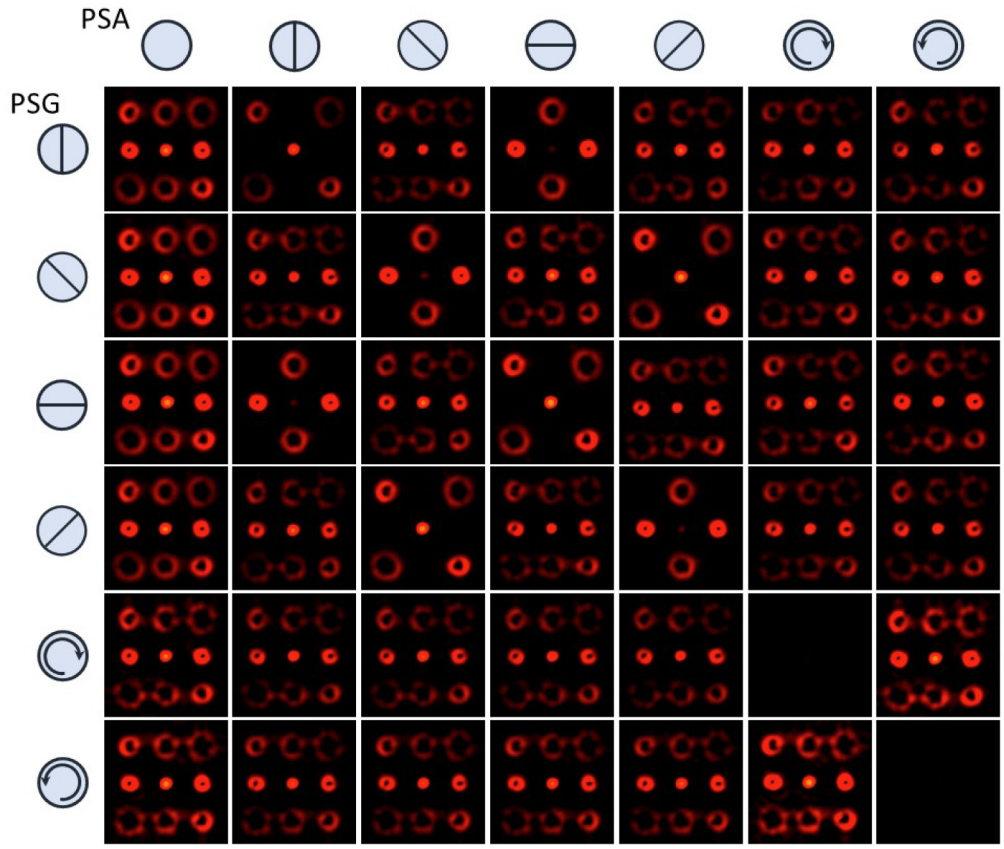

Fig. 6. Experimental results of the Fourier plane for six different configurations of the PSG without analyzer (left column), and with six different configurations of the PSA.

The left column of CCD captures in Fig. 6 shows the diffracted pattern when no analyzer is included. In all cases, the 3 × 3 vortex beam array is successfully obtained. However, the polarization of each order changes, and this is noticeable when the PSA is included and configured to detect different states. When the grating is illuminated with linearly polarized light (results in the first four rows in Fig. 6), we can identify two sets of diffraction orders with different polarization, as expected from the discussion in Section 3. According to Eq. (18), the zero order and the diagonal orders experience a polarization transformation with respect to the input polarization equivalent to that caused by a half-wave retarder oriented along the x-y axes. On the contrary, those orders diffracted in the x and y directions ((1,0), (0,1), (–1,0) and (0,-1)) transform the input polarization states as if they traversed a polarization rotator of 90° followed by an aligned half-wave retarder.

These polarization changes can be clearly noticed in the first row of results. Since the input light is vertical linearly polarized, the first set of five orders exit the grating with the same vertical polarization, while the other four orders exit with horizontal linear polarization. This is shown by the extinction of the two set of orders when the PSA is configured vertical and horizontal respectively. On the contrary, when the PSA is linear at ± 45° or circular all nine orders are visible. The other cases when the grating is illuminated with a linear state confirm these results. Note that these polarization changes arise from the relative $\pi/2$ phase shift between the zero order and the ± 1 orders in Gori's triplicator design. Note that the different polarization behavior in these two sets of diffraction orders was also observed in a recently reported 2D grating design [24]. Although the design in that work is different to ours,

Optics EXPRESS

it also includes the product of two triplicators in the *x*-*y* directions, and therefore the relative $\pi/2$ phase shift is expected to play also a role.

The situation is different when circularly polarized light illuminates the grating, as shown in the two bottom rows in Fig. 6. Here the grating acts as a pure geometric phase grating, imparting the encoded spatial phase, but the change in polarization in both cases is uniform to all orders and consists in a change of helicity of the circular polarization (input right circular polarization is transformed into left, and viceversa). This is shown by the fact that all diffraction orders are visible when the PSA is set to detect linear states. When it is configured to detect the circular states, the state equal to the input one is completely cancelled, while the opposite is fully transmitted.

As a final result, we examine the use of the GP vortex grating as a vortex beam detector. For that purpose, we include a *q*-plate behind the PSG. When the PSG is set to generate a circular polarization state, the *q*-plate output is a vortex beam with topological charge ± 2*q* and the opposite circular polarization. Figure 7 shows the results captured at the Fourier plane when we illuminate the vortex grating with the output from a *q*-plate with $q = 1/2$ for two cases.

In Fig. 7(a) the *q*-plate is illuminated with R circular polarization, so its output is a vortex beam with L circular polarization and topological charge $\ell_{in} = +1$. This input charge is compensated on the diffraction order having charge $\ell = -1$ and therefore a bright spot on the (−1,0) order appears. In the second case in Fig. 7(b), the *q*-plate is illuminated with L circular polarization, and now the beam impinging on the grating is a vortex beam with R circular polarization and topological charge $\ell_{in} = -1$. Now the bright spot appears on the (+ 1,0) diffraction order where the grating generates the vortex beam with charge $\ell = +1$. These results show that the grating could be used also as a vortex beam detector, although now the resolution limits are clearly visible in the distortion of the orders having higher topological charges.

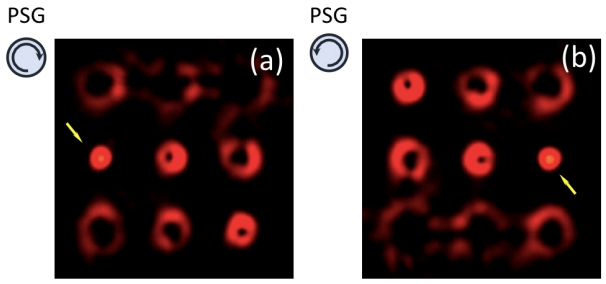

Fig. 7. Experimental results at the Fourier plane for the 2D vortex grating illuminated with two circularly polarized vortex beams of charges (a) + 1 (b) −1. No PSA is included. The yellow arrow indicates the position of the bright spot, revealing the input charge.

5. Conclusions

In summary, we have proposed, analyzed and demonstrated the application of the triplicator phase profile to a 2D vortex diffraction grating. We completed Gori's et al analysis in [3] by showing the $\pi/2$ relative phase between the zero and the ± 1 diffraction orders, which is key to render different polarization at two sets of diffraction orders. We designed the 2D vortex triplicator grating and ordered its fabrication as a geometric-phase liquid-crystal grating by using a commercially available capability offered to fabricate customized retarders. The fabricated grating has been evaluated experimentally and confirms the theoretical predictions.

This grating is an interesting diffractive element since, when being illuminated with a plane wave, it creates a bidimensional array of 3 × 3 vortex beams of integer topological charges ranging from + 4 to −4, and with the optimal diffraction efficiency. The same grating

Optics EXPRESS

could be used also as a detector of vortex beams, where the charge is detected by seeking the diffraction order where the singularity is cancelled [26]. The advantage of the triplicator design relies on its optimal diffraction efficiency, which might be of great importance in applications with low light intensity levels.

Finally, we have shown an experimental proof-of concept using a commercial capability to fabricate customized non-standard geometric-phase diffraction gratings. Despite the limited spatial resolution, this opens interesting possibilities to researchers in the field who do not have facilities to fabricate such geometric-phase elements.

Appendix

In this Appendix we review the derivation of Gori's triplicator and derive the condition in Eq. (5), which we have shown to be the cause of the different polarization behavior at different diffraction orders. The coefficients for the Fourier expansion of the optimum triplicator are calculated for the 0,+1 and −1 terms.

The zero order in the Fourier expansion of the optimal triplicator in Eq. (1) takes the form:

$$\tau_0 = \frac{1}{p}\int_{-p/2}^{p/2} \exp\left[i\phi(x)\right]dx = \frac{1}{p}\int_{-p/2}^{p/2} \exp\left[\arctan\left(a\cos\left(\frac{2\pi x}{p}\right)\right)\right]dx. \tag{19}$$

If the change of variable $\delta = 2\pi x/p$ is applied, Eq. (19) is reduced to

$$\tau_0 = \frac{1}{2\pi}\int_{-\pi}^{\pi} \exp\left[\arctan\left(a\cos\delta\right)\right]d\delta, \tag{20}$$

which is expanded in two integrals by applying Euler's formula

$$\tau_0 = \frac{1}{2\pi}\int_{-\pi}^{\pi} \cos\left[\arctan\left(a\cos\delta\right)\right]d\delta + \frac{i}{2\pi}\int_{-\pi}^{\pi} \sin\left[\arctan\left(a\cos\delta\right)\right]d\delta. \tag{21}$$

These two integrals can be calculated using the trigonometric relations

$$\cos\left(\arctan\varphi\right) = \frac{1}{\sqrt{1+\varphi^2}}, \tag{22}$$

$$\sin\left(\arctan\varphi\right) = \frac{\varphi}{\sqrt{1+\varphi^2}}, \tag{23}$$

so Eq. (21) can be rewritten as

$$\tau_0 = \frac{1}{2\pi}\int_{-\pi}^{\pi} \frac{1}{\sqrt{1+a^2\cos^2\delta}}d\delta + \frac{i}{2\pi}\int_{-\pi}^{\pi} \frac{a\cos\delta}{\sqrt{1+a^2\cos^2\delta}}d\delta, \tag{24}$$

Since both integrals are even functions they can be written as

$$\tau_0 = \frac{1}{\pi}\int_{0}^{\pi} \frac{1}{\sqrt{1+a^2\cos^2\delta}}d\delta + \frac{i}{\pi}\int_{0}^{\pi} \frac{a\cos\delta}{\sqrt{1+a^2\cos^2\delta}}d\delta, \tag{25}$$

But note that the second integral in Eq. (25) is antisymmetric around the value $\delta = \pi/2$, and therefore it vanishes. Consequently, τ_0 is a pure real and positive value given by

$$\tau_0 = \frac{1}{\pi}\int_{0}^{\pi} \frac{1}{\sqrt{1+a^2\cos^2\delta}}d\delta = \frac{2}{\pi}K\left(-a^2\right), \tag{26}$$

Optics EXPRESS

where K is the complete elliptic integral of the first kind. For the numerical constant a = 2.65718 derived in the triplicator design [3], the zero order coefficient τ_0 is 0.555.

Next, let us calculate the coefficients for the +1 and −1 orders. In this case

$$\tau_{\pm 1} = \frac{1}{p}\int_{-p/2}^{p/2} \exp\left[\arctan\left(a\cos\left(\frac{2\pi x}{p}\right)\right)\right]\exp\left(\pm i\frac{2\pi x}{p}\right)dx, \tag{27}$$

If the change of variable $\delta = 2\pi x/p$ is again applied, Eq. (2) reduces to

$$\tau_{\pm 1} = \frac{1}{2\pi}\int_{-\pi}^{\pi} \exp\left[\arctan\left(a\cos\delta\right)\right]\exp\left(\pm i\delta\right)d\delta. \tag{28}$$

Applying Euler formula to each exponential function in Eq. (28), four different terms are obtained

$$\begin{aligned}\tau_{\pm 1} = &\frac{1}{2\pi}\int_{-\pi}^{\pi}\cos\left(\arctan\left(a\cos\delta\right)\right)\cos\delta\, d\delta + \\ &\mp\frac{1}{2\pi}\int_{-\pi}^{\pi}\sin\left(\arctan\left(a\cos\delta\right)\right)\sin\delta\, d\delta + \\ &\pm\frac{i}{2\pi}\int_{-\pi}^{\pi}\cos\left(\arctan\left(a\cos\delta\right)\right)\sin\delta\, d\delta + \\ &+\frac{i}{2\pi}\int_{-\pi}^{\pi}\sin\left(\arctan\left(a\cos\delta\right)\right)\cos\delta\, d\delta,\end{aligned} \tag{29}$$

and considering Eqs. (22) and (23), the following decomposition is obtained

$$\begin{aligned}\tau_{\pm 1} = &\frac{1}{2\pi}\int_{-\pi}^{\pi}\frac{\cos\delta}{\sqrt{1+a^2\cos^2\delta}}d\delta \mp \frac{1}{2\pi}\int_{-\pi}^{\pi}\frac{a\cos\delta\sin\delta}{\sqrt{1+a^2\cos^2\delta}}d\delta + \\ &\pm\frac{i}{2\pi}\int_{-\pi}^{\pi}\frac{\sin\delta}{\sqrt{1+a^2\cos^2\delta}}d\delta + \frac{i}{2\pi}\int_{-\pi}^{\pi}\frac{a\cos^2\delta}{\sqrt{1+a^2\cos^2\delta}}d\delta.\end{aligned} \tag{30}$$

Now, the same kind of symmetry considerations can be applied to these four terms. The second and third terms are odd functions about zero, so their definite integrals are zero. And the first and fourth terms in the sum are both even functions about zero, so its definite integral can be expressed as twice the integral from 0 to π., i.e.

$$\tau_{\pm 1} = \frac{1}{\pi}\int_{0}^{\pi}\frac{\cos\delta}{\sqrt{1+a^2\cos^2\delta}} + \frac{i}{\pi}\int_{0}^{\pi}\frac{a\cos^2\delta}{\sqrt{1+a^2\cos^2\delta}}d\delta. \tag{31}$$

Then, by noticing that the first term is an odd function about π/2, this first integral turns to be also zero, and the only remaining term is the fourth term, which is given by

$$\tau_{\pm 1} = \frac{ia}{\pi}\int_{0}^{\pi}\frac{\cos^2\delta}{\sqrt{1+a^2\cos^2\delta}}d\delta = i\frac{2}{\pi a}\left[E\left(-a^2\right) - K\left(-a^2\right)\right], \tag{32}$$

where E denotes the complete elliptic integral of the second kind. Note that both orders get the same pure positive imaginary value. For a = 2.65718, this value is $\tau_{\pm 1} = 0.555i$.

Optics EXPRESS

Funding

Conselleria d'Educació, Investigació, Cultura i Esport (PROMETEO-2017-154); Ministerio de Economía y Competitividad (FIS2015-66328-C3-3-R); Fondo Nacional de Desarrollo Científico y Tecnológico, Chile (FONDECYT) (1151290).

References

1. H. Dammann and E. Klotz, "Coherent optical generation and inspection of two-dimensional periodic structures," Opt. Acta (Lond.) **24**(4), 505–515 (1977).
2. J. N. Mait, "Design of binary-phase and multiphase Fourier gratings for array generation," J. Opt. Soc. Am. A **7**(8), 1514–1518 (1990).
3. F. Gori, M. Santarsiero, S. Vicalvi, R. Borghi, G. Cincotti, E. di Fabrizio, and M. Gentili, "Analytical derivation of the optimum triplicator," Opt. Commun. **157**(1-6), 13–16 (1998).
4. F. Aroca and I. Moreno, "Comparison and experimental realization of different phase-only grating designs and optimal triplicators," Opt. Pura Apl. **49**(3), 155–166 (2016).
5. A. Cofré, P. García-Martínez, A. Vargas, and I. Moreno, "Vortex beam generation and other advanced optics experiments reproduced with a twisted-nematic liquid-crystal display with limited phase modulation," Eur. J. Phys. **38**(1), 014005 (2017).
6. L. A. Romero and F. M. Dickey, "The mathematical theory of laser beam-splitting gratings," Prog. Opt. **54**, 319–386 (2010).
7. A. V. Carpentier, H. Michinel, J. R. Salgueiro, and D. Olivieri, "Making optical vortices with computer-generated holograms," Am. J. Phys. **76**(10), 916–921 (2008).
8. I. Moreno, J. A. Davis, D. M. Cottrell, N. Zhang, and X.-C. Yuan, "Encoding generalized phase functions on Dammann gratings," Opt. Lett. **35**(10), 1536–1538 (2010).
9. T. Lei, M. Zhang, Y. Li, P. Jia, G. N. Liu, X. Xu, Z. Li, C. Min, J. Lin, C. Yu, H. Niu, and X. Yuan, "Massive individual orbital angular momentum channels for multiplexing enabled by Dammann gratings," Light Sci. Appl. **4**(3), e257 (2015).
10. J. A. Davis, D. M. Cottrell, K. R. McCormick, J. Albero, and I. Moreno, "Arithmetic of focused vortex beams in three-dimensional optical lattice arrays," Appl. Opt. **53**(10), 2040–2050 (2014).
11. C. Maurer, A. Jesacher, S. Fürhapter, S. Bernet, and M. Ritsch-Marte, "Tailoring of arbitrary optical vector beams," New J. Phys. **9**(3), 78 (2007).
12. I. Moreno, J. A. Davis, K. Badham, M. M. Sánchez-López, J. E. Holland, and D. M. Cottrell, "Vector beam polarization state spectrum analyzer," Sci. Rep. **7**(1), 2216 (2017).
13. C. Rosales-Guzmán, N. Bhebhe, and A. Forbes, "Simultaneous generation of multiple vector beams on a single SLM," Opt. Express **25**(21), 25697–25706 (2017).
14. F. Yue, D. Wen, C. Zhang, B. D. Gerardot, W. Wang, S. Zhang, and X. Chen, "Multichannel polarization-controllable superpositions of orbital angular momentum states," Adv. Mater. **29**(15), 1603838 (2017).
15. J. Kim, Y. Li, M. N. Miskiewicz, C. Oh, M. W. Kudenov, and M. J. Escuti, "Fabrication of ideal geometric-phase holograms with arbitrary wavefronts," Optica **2**(11), 958–964 (2015).
16. L. De Sio, D. E. Roberts, Z. Liao, S. Nersisyan, O. Uskova, L. Wickboldt, N. Tabiryan, D. M. Steeves, and B. R. Kimball, "Digital polarization holography advancing geometrical phase optics," Opt. Express **24**(16), 18297–18306 (2016).
17. P. Chen, Y.-Q. Lu, and W. Hu, "Beam shaping via photopatterned liquid crystals," Liq. Cryst. **43**(13–15), 2051–2061 (2016).
18. P. Chen, B.-Y. Wei, W. Ji, S.-J. Ge, W. Hu, F. Xu, V. Chigrinov, and Y.-Q. Lu, "Arbitrary and reconfigurable optical vortex generation: A high-efficiency technique using director-varying liquid crystal fork gratings," Photon. Res. **3**(4), 133–139 (2015).
19. P. Chen, L.-L. Ma, W. Duan, J. Chen, S.-J. Ge, Z.-H. Zhu, M.-J. Tang, R. Xu, W. Gao, T. Li, W. Hu, and Y.-Q. Lu, "Digitalizing self-assembled chiral superstructures for optical vortex processing," Adv. Mater. **30**(10), 1705865 (2018).
20. J. P. Balthasar Mueller, N. A. Rubin, R. C. Devlin, B. Groever, and F. Capasso, "Metasurface polarization optics: independent phase control of arbitrary orthogonal states of polarization," Phys. Rev. Lett. **118**(11), 113901 (2017).
21. M. Beresna, M. Gecevičius, P. G. Kazansky, and T. Gertus, "Radially polarized optical vortex converter created by femtosecond laser nanostructuring of glass," Appl. Phys. Lett. **98**(20), 201101 (2011).
22. A. Cofré, A. Vargas, F. A. Torres-Ruíz, M. M. Sánchez-López, and I. Moreno, "Geometrical-phase lens based optical system for the spin-splitting of vector beams," Opt. Lasers Eng. **110**, 401–409 (2018).
23. https://www.thorlabs.com/newgrouppage9.cfm?objectgroup_id=9098
24. M. Yannai, E. Maguid, A. Faerman, Q. Li, J.-H. Song, V. Kleiner, M. L. Brongersma, and E. Hasman, "Spectrally interleaved topologies using geometric phase metasurfaces," Opt. Express **26**(23), 31031–31038 (2018).
25. C. Zhou and L. Liu, "Numerical study of Dammann array illuminators," Appl. Opt. **34**(26), 5961–5969 (1995).
26. I. Moreno, J. A. Davis, B. M. L. Pascoguin, M. J. Mitry, and D. M. Cottrell, "Vortex sensing diffraction gratings," Opt. Lett. **34**(19), 2927–2929 (2009).

Optics EXPRESS

27. P. Chen, S.-J. Ge, L.-L. Ma, W. Hu, V. Chigrinov, and Y.-Q. Lu, "Generation of equal-energy orbital angular momentum beams via photopatterned liquid crystals," Phys. Rev. Appl. **5**(4), 044009 (2016).
28. Z. Xie, T. Lei, X. Weng, L. Du, S. Gao, Y. Yuan, S. Feng, Y. Zhang, and X. Yuan, "A miniaturized polymer grating for topological order detection of cylindrical vector beams," IEEE Photonics Technol. Lett. **28**(24), 2799–2802 (2016).
29. P. Chen, S.-J. Ge, W. Duan, B.-Y. Wei, G.-X. Cui, W. Hu, and Y.-Q. Lu, "Digitalized geometric phases for parallel optical spin and orbital angular momentum encoding," ACS Photonics **4**(6), 1333–1338 (2017).
30. L. Marrucci, C. Manzo, and D. Paparo, "Optical spin-to-orbital angular momentum conversion in inhomogeneous anisotropic media," Phys. Rev. Lett. **96**(16), 163905 (2006).